International Journal of Bifurcation and Chaos, Vol. 21, No. 3 (2011) 869–884

DOI: 10.1142/S0218127411028854

REGULAR AND CHAOTIC DYNAMICS IN BOUNCING BALL MODELS

SEBASTIAN VOGEL* and STEFAN J. LINZ†
Institut für Theoretische Physik,
Westfälische Wilhelms-Universität Münster,
Wilhelm-Klemm-Str. 9, 48149 Münster, Germany
**Sebastian.Vogel@uni-muenster.de*
†*slinz@uni-muenster.de*

Received September 20, 2010

One of the prime paradigms for complex temporal dynamics, the motion of an inelastic ball bouncing on a sinusoidally oscillating table, is revisited. Using extensive numerical simulations, we address the not yet conclusively settled problem of the occurrence of chaos in the partially elastic case. We systematically investigate the spectrum of long-time solutions as function of the initial conditions and system parameters. Subsequently, we generalize the bouncing ball system by taking the velocity dependence of the coefficient of restitution into account and exemplarily demonstrate the drastic impact of such a generalization on the overall dynamics.

Keywords: Bouncing ball models; periodic and chaotic solutions; Lyapunov exponents; attractors; energy dissipation and driving.

1. Introduction

The bouncing ball system has been the subject of intense studies both in experiments and theory during the past decades. It consists of a point-like particle bouncing on a vertically and sinusoidally oscillating table. Conceptionally simple, it has revealed a plethora of diverse dynamical behavior and has become one of the prototypical examples in nonlinear dynamics and chaos theory.

In addition, it has proven to be valuable for understanding more complex systems, such as probability machines [Hansen *et al.*, 1995], particle transport on conveyor belts [El hor & Linz, 2005], quantum billiard [Stöckmann, 2007], and chaos control [Vargas *et al.*, 2009]. Its history can be traced back to a paper by Fermi [1949] and it started to become prominent over three decades ago [Zaslavskii, 1978]. For an overview of the extensive literature on the subject, we refer the reader to the references given at the end of this paper and — especially for the early literature — to the article by Lichtenberg *et al.* [1980] and the book by Tufillaro *et al.* [1992].

The main aim of this paper is to review the properties of the bouncing ball system in detail. We also investigate some of the questions that have not yet been sufficiently clarified. For example, some authors [Pierański *et al.*, 1985; Tufillaro & Albano, 1986; Tufillaro *et al.*, 1986; Celaschi & Zimmermann, 1987; Mello & Tufillaro, 1987; Tufillaro, 1994a, 1994b; Kowalik *et al.*, 1988] have observed period-doubling and chaos in the bouncing ball system, whereas others believe that "the period-doubling route to chaos should not be observed" and "a generic trajectory of the partially elastic bouncing ball is eventually periodic" [Luck & Mehta, 1993]. Furthermore, no overall systematic investigation of the long-term behavior of the bouncing ball problem depending on initial conditions and parameters has been presented yet.

We address these questions in the first part of this paper after reviewing the standard theoretical model for the bouncing ball. In the course of the investigation, we will answer the question of existence of chaos in a positive way. A scan of all accessible parameters will show that chaotic solutions, although present, are not dominating the parameter space. In the larger part of the parameter space, sticking solutions do prevail.

Usually, when modeling the bouncing ball system, the ball is approximated as a point particle, air friction is excluded, and impacts are supposed to happen instantaneously without affecting the oscillations of the table. The motion of the ball is restricted to the vertical direction by assuming a perfectly planar table. Hence, until now almost all theoretical models have completely neglected, or included only in an approximative way [Luna-Acosta, 1990], a number of physical effects which can be expected to play a vital role in experiments. To our knowledge, the only in-depth investigation was done by Naylor *et al.* [2002] concerning the relevance of air friction.

For this reason, in the second part of this paper we examine the influence of one of the hitherto neglected effects, namely the velocity dependence of the coefficient of restitution. This effect will always be present, even if experiments are performed under vacuum conditions. It will turn out that changes are crucial and care should be taken when comparing theoretical findings with experiments. The final section of this paper is devoted to the examination of average jump heights of the ball above the table.

2. Basics

2.1. *Basic equations*

The trajectory of the ball between impacts is completely determined by Newton's law. It is therefore sufficient to consecutively identify the impact times t_i and lift-off velocities v_i of the ball immediately after the ith impact of the ball on the table. Velocities in the laboratory frame will be called absolute velocities and velocities in the comoving frame of the table relative velocities. Let δ_0 be the offset at $t = 0, \omega$ the angular frequency, and A the amplitude of the oscillations of the table $x = A\sin(\omega t + \delta_0)$. The incoming velocity v_i' and the outgoing velocity v_i are linked via the so-called impact relation

$$v_i = (1+\epsilon)s_i - \epsilon v_i', \tag{1}$$

where $s_i = A\omega\cos(\omega t_{i+1} + \delta_0)$ denotes the velocity of the table at time t_{i+1} and ϵ the coefficient of restitution. A straightforward calculation yields (for details, see for example [Tufillaro *et al.*, 1992]) a system of coupled iterated maps for the time evolution of t_i and v_i

$$0 = A\sin(\omega t_i + \delta_0) + v_i\,(t_{i+1} - t_i) - \frac{1}{2}g(t_{i+1} - t_i)^2 - A\sin(\omega t_{i+1} + \delta_0) \tag{2}$$

$$v_{i+1} = (1+\epsilon)A\omega\cos(\omega t_{i+1} + \delta_0) - \epsilon[v_i - g(t_{i+1} - t_i)], \tag{3}$$

where the successive impact times t_{i+1} result from the implicit Eq. (2). It is often convenient to switch to dimensionless quantities, namely to a normalized time $\tau = (\omega t + \delta_0)/2\pi$ (or $\phi = \tau \bmod 1$, whenever only the phase of the oscillations of the table is relevant), a relative lift-off velocity

$$W = \frac{[v - A\omega\cos(\omega t + \delta_0)]\omega}{\pi g}, \tag{4}$$

and a normalized acceleration or driving strength

$$\Gamma = \frac{A\omega^2}{g}. \tag{5}$$

Heights X will be expressed in units of $2\pi^2 g/\omega^2$. Apart from a factor of $1/\pi$ in Γ our notation is equivalent to the one introduced in the papers by Mehta and Luck [1990], Luck and Mehta [1993]. The two-dimensional system of difference equations (2)–(3) then reads

$$0 = \frac{\Gamma}{2\pi^2}[\sin(2\pi\tau_i) - \sin(2\pi\tau_{i+1})] + \left[W_i + \frac{\Gamma}{\pi}\cos(2\pi\tau_i)\right](\tau_{i+1} - \tau_i) - (\tau_{i+1} - \tau_i)^2 \tag{6}$$

$$W_{i+1} = -\epsilon\left\{W_i - 2(\tau_{i+1} - \tau_i) + \frac{\Gamma}{\pi}[\cos(2\pi\tau_i) - \cos(2\pi\tau_{i+1})]\right\}. \tag{7}$$

In numerical computations the only difficult task is to solve Eq. (2) or equivalently Eq. (6). In accordance with most of the work done in the literature, we employed the bisection method to this purpose. Our numerical calculations are all based on

the system of Eqs. (2)–(3). This makes our results more amenable to a direct comparison with experimental data and the larger part of the published theoretical findings. However, in this paper we generally present our results in dimensionless units. Hereby, the number of parameters can be limited to two, i.e. the coefficient of restitution ϵ and the normalized acceleration Γ. Initial conditions are ϕ_0 and W_0.

2.2. *Types of solutions*

Experimentally and theoretically three different types of solutions can be distinguished in the long-term limit. We give a short review.

2.2.1. *Periodic solutions*

In some regions of parameter space periodic solutions can be initiated by a suitable choice of initial conditions. In Fig. 1(a) the ball ends up repeating a series consisting of a high jump followed by a lower jump forever after completing a transient regime, i.e. in an orbit of period two. For one-periodic orbits (not shown in the figure) the phase and lift-off velocity as well as their region of stability can be calculated analytically. To our knowledge this was first done by Pippard [1989]. For the region of stability one gets

$$\frac{1-\epsilon}{1+\epsilon}\pi m \le \Gamma \le \pi\left\{\left[\frac{1-\epsilon}{1+\epsilon}m\right]^2 + \left[\frac{2(1+\epsilon^2)}{\pi(1+\epsilon)^2}\right]^2\right\}^{\frac{1}{2}}. \tag{8}$$

Here, m denotes the number of oscillations of the table between subsequent impacts.

2.2.2. *Chaotic orbits*

We mentioned in the introduction that the existence of chaos in the bouncing ball system is still a matter of debate. In any case, orbits which at first sight do not exhibit any sign of periodicity, do exist. The first few impacts of such a representative orbit are shown in Fig. 1(b). A more in-depth analysis can be found in Secs. 3.1–3.3 of this paper.

2.2.3. *Sticking solutions*

If the downward acceleration of the table is smaller than gravity and the relative velocity of the incoming ball is low enough, it may perform a number of smaller and smaller jumps before getting completely stuck on the table. Numerical and theoretical work has been done by Luck and Mehta [1993] concerning the size and relevance of this so-called "locking region" in phase space. No analytic expression could be derived for it until now. After getting stuck, the ball will either constantly stick to the table ($\Gamma \le 1$) or lift off again at the point given by $\phi = \arcsin(1/\Gamma)/2\pi$ with zero relative velocity ($\Gamma > 1$). Whenever the ball gets stuck at least twice, such an orbit is called a sticking solution. Otherwise, we speak of free solutions. From an analytical point of view sticking solutions are always periodic of nature, due to identical lift-off conditions (see, however, Sec. 3.1).

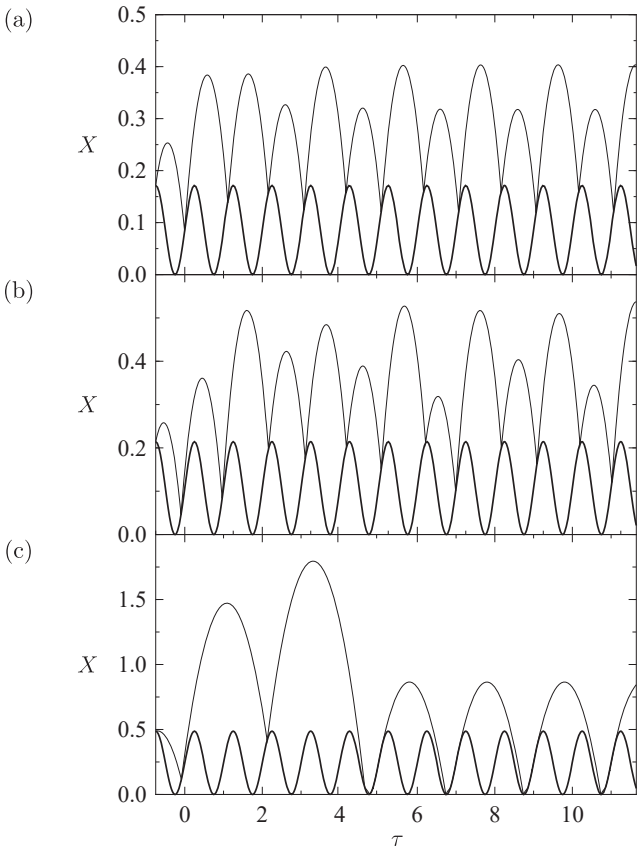

Fig. 1. Representative time evolution of different types of solutions in the bouncing ball system. Trajectories of the ball: thin line —, motion of the table: thick line —. (a) Periodic solution. (b) Chaotic solution. (c) Sticking solution.

2.3. *Trapping region*

Obviously, a lower bound for the outgoing velocity of the ball is given by the minimum velocity of the table $W = 0$ or $v = -A\omega$. For $\epsilon < 1$ an upper limit for the outgoing velocity of the ball can also

be derived, indicating (apart from transients) the upper bound of this so-called trapping region for the velocity of the ball. Tufillaro *et al.* [1992] have shown that

$$V^T_{\max} = \frac{(1+3\epsilon)\Gamma}{(1-\epsilon)\pi}, \tag{9}$$

where $V^T_{\max}$ is an absolute velocity expressed in units of $\pi g/\omega$. Another result in relative quantities has been put forward by Luck and Mehta [1993]

$$W^{LM}_{\max} = \frac{\epsilon}{1-\epsilon^2}\left\{(3+\epsilon)\frac{\Gamma}{\pi} + \left[4(1-\epsilon^2)\frac{\Gamma}{\pi^2} + (1+3\epsilon)^2\frac{\Gamma^2}{\pi^2}\right]^{\frac{1}{2}}\right\}. \tag{10}$$

Here, we present a third and novel result which will prove more accurate for some purposes. As starting point, we choose Eq. (1). The speed of the table s_i can always be restricted to its maximum value $A\omega$. Moreover, the difference in height between two consecutive impacts can amount to no more than $2A$. This fact establishes a link between the outgoing velocity v_i and the maximum incoming velocity v'_{i+1}. Equation (1) hence reads

$$v_{i+1} \le (1+\epsilon)A\omega + \epsilon(v_i + 2\sqrt{gA}). \tag{11}$$

By means of induction, we obtain

$$v_{i+1} \le \sum_{l=0}^{k-1}\epsilon^l(1+\epsilon)A\omega + \sum_{l=0}^{k-1}\epsilon^{l+1}2\sqrt{gA} + \epsilon^k v_{i-k+1}. \tag{12}$$

In the long-term limit this reduces to

$$v_{i+1} \le v^*_{\max} = \frac{(1+\epsilon)A\omega + 2\epsilon\sqrt{gA}}{1-\epsilon}, \tag{13}$$

which can be written in dimensionless units as

$$V^*_{\max} = \frac{(1+\epsilon)\Gamma + 2\epsilon\sqrt{\Gamma}}{(1-\epsilon)\pi} \tag{14}$$

and shows that for nonelastic balls $\epsilon < 1$ there is always a finite bound $V^*_{\max}$.

To compare the three different results, $V^T_{\max}$, $W^{LM}_{\max}$ and $V^*_{\max}$, we first note that the difference between $V^T_{\max}$ and $V^*_{\max}$ amounts to

$$V^T_{\max} - V^*_{\max} = \frac{2\epsilon(\Gamma - \sqrt{\Gamma})}{(1-\epsilon)\pi}. \tag{15}$$

This relation proves that $V^T_{\max} < V^*_{\max}$ only for $\Gamma < 1$.

The comparison with $W^{LM}_{\max}$ needs slightly more thought, since the transition from relative to absolute quantities and vice versa is now no longer symmetrical. Obviously, in the first case (transition from relative to absolute velocities) one has to add the maximum table velocity $\Gamma/\pi = (A\omega)\cdot(\omega/\pi g)$ to the relative velocity $W^{LM}_{\max}$, which yields $V^{LM}_{\max} = W^{LM}_{\max} + (\Gamma/\pi)$. In the second case (transition from absolute to relative velocities) Γ/π also has to be added to — not subtracted from — the absolute velocities $V^*_{\max}$ or $V^T_{\max}$. In Sec. 2.1 we have pointed out that our computational algorithms rely on absolute velocities. Therefore, we limit ourselves in this paper to a comparison for absolute velocities.

Calculations can be shortened by neglecting the first, always positive term of the radiant in Eq. (10). One obtains

$$V^{LM}_{\max} = W^{LM}_{\max} + \frac{\Gamma}{\pi} \ge \frac{(1+3\epsilon)\Gamma}{(1-\epsilon)\pi}. \tag{16}$$

Since the right-hand side of Eq. (16) is equal to $V^T_{\max}$, it follows that in the laboratory frame $V^T_{\max}$ is the most accurate upper bound for the outgoing velocity of the ball for $\Gamma < 1$. $V^*_{\max}$ constitutes a stricter bound for the case $\Gamma > 1$.

3. Constant Coefficient of Restitution

3.1. *Bifurcation diagrams and Lyapunov exponents*

As a first step it is instructive to fix ϵ and vary only the driving Γ. To obtain the graph shown in Fig. 2(a) we proceeded as follows: at the lowest visible Γ-value we initiated a sequence of jumps starting from the initial conditions (ϕ_0, W_0) indicated in the figure caption. We did not take into account the first 20 000 impacts in order to eliminate transients. We next plotted the impact phase ϕ for the subsequent 30 000 impacts. Finally, we slightly increased Γ and used the last values $(\phi_{50\,000}, U_{50\,000})$ as new initial conditions. In experiments, this conforms to letting the ball jump on the table while

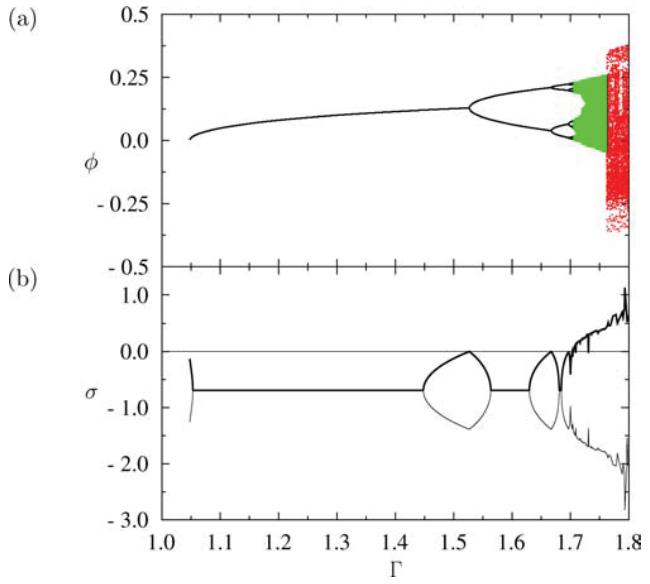

Fig. 2. (a) Bifurcation diagram for $\epsilon = 0.5$. Black: regular solutions, red: sticking solutions, green: chaotic solutions. $\phi_0 = 0, W_0 = 2/3$ at $\Gamma = 1.03$. (b) Corresponding Lyapunov exponents σ_1 ——, σ_2 ——. Also shown is the zero-line.

adiabatically increasing the strength of the table's oscillations. We employed the same procedure for all bifurcation diagrams in this paper, except for the ones shown in Fig. 4.

Bifurcation cascades such as in Fig. 2(a) are well known from the literature [Tufillaro *et al.*, 1992; Tufillaro, 1994a, 1994b; Celaschi & Zimmermann, 1987] and can also be observed in experiments for a limited parameter range [Pierański *et al.*, 1985; Pippard, 1989; Zimmermann *et al.*, 1992; Pierański, 1988; Pierański & Malecki, 1986]. Because of the observable period doubling route to chaos it is no surprise to find also chaotic behavior, in Fig. 2 between $\Gamma \approx 1.7$ and $\Gamma \approx 1.76$. Generally, the existence of a positive Lyapunov exponent is a strong evidence for chaos, indicating that neighboring phase-space trajectories diverge exponentially fast. In Fig. 2(b) we therefore plotted the associated Lyapunov exponents σ_1 and σ_2, where $\sigma_1 < \sigma_2$. To our knowledge only two values for Lyapunov exponents for a sinusoidally oscillating table have been published before by Oliveira and Gonçalves [1997]. Despite extensive checks we could not reproduce their values.

It is, however, obvious from Fig. 2 that our results do within computational accuracy agree with mandatory features that can be derived analytically: both exponents are negative for stable periodic orbits; at bifurcation points one correctly obtains $\sigma_2 = 0$. In addition, the constant baseline, around which σ_1 and σ_2 are arranged symmetrically, can also be explained theoretically. This feature is well known from two-dimensional systems with $|\det D_i(\mathbf{x}_i)| = \nu = \text{const.}$, e.g. the Hénon map [Hénon, 1976; Klein, 1992] and the bouncing ball in Everson's high-bounce approximation [Everson, 1986]. Here, $\det D_i(\mathbf{x}_i)$ denotes the functional determinant of a two-dimensional system of difference equations describing the evolution of the model system at time i. In this case, the sum of the two Lyapunov exponents amounts to

$$\sigma_1 + \sigma_2 = \ln \nu, \tag{17}$$

explaining the symmetry. Moreover, Lyapunov exponents can be calculated from the absolute values of eigenvalues of the matrices $\mathbf{J}_i = \prod_{k=0}^{i-1} D_k(\mathbf{x}_k)$. These are either real or complex conjugate, where the latter case explains the regions with a constant baseline. Finally, Eq. (17) remains valid under the weaker condition $|\det \mathbf{J}_i| = \nu^i \cdot c(i)$, where $\nu > 0$ is a real number and $c(i)$ is a positive valued discrete and bounded function. In our case, the relevant system of difference equations is given by Eqs. (6) and (7) where $\mathbf{x}_i = (\phi_i, W_i)$. After some calculations we get

$$\det D_i \begin{pmatrix} \phi_i \\ W_i \end{pmatrix} = \epsilon^2 \frac{W_i}{W_{i+1}} \tag{18}$$

and hence

$$\det \mathbf{J}_i = \epsilon^{2i} \frac{W_0}{W_i}. \tag{19}$$

Therefore, the weaker condition is fulfilled with $\nu = \epsilon^2$ and $c(i) = W_0/W_i$. The constant baseline in Figs. 2(b) and 3(b) is given by $\ln \epsilon$.

The fact that σ_2 becomes positive above $\Gamma \approx 1.7$ in Fig. 2 gives strong evidence for the existence of chaos. A more detailed view of that region, which is not shown here, reveals that other features such as periodic windows are mirrored correctly by the sign of σ_2. As it will turn out, however, Lyapunov exponents alone are not sufficient to unambiguously identify chaotic behavior.

If the acceleration is increased above $\Gamma \approx 1.76$, the ball abruptly changes its behavior from free jumps to sticking solutions. We also calculated Lyapunov exponents for sticking solutions. Since an infinite number of jumps occurs during the sticking process, it is not evident how Lyapunov exponents

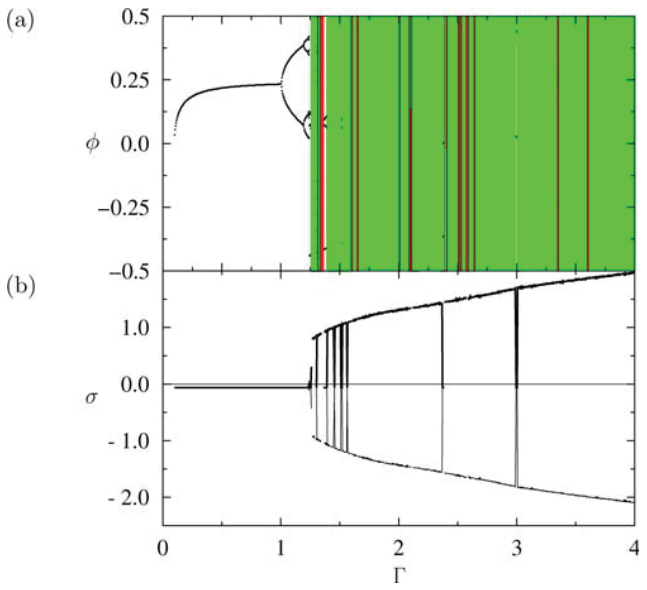

Fig. 3. (a) Bifurcation diagram for $\epsilon = 0.94$. Black: regular solutions, red: sticking solutions, green: chaotic solution. $\phi_0 = 0, W_0 = 0.9582$ at $\Gamma = 0.35$. (b) Corresponding Lyapunov exponents σ_1 —, σ_2 —. Also shown is the zero-line.

can reasonably be defined for sticking solutions at all. Therefore, we proceeded the following way: orbits where less than 100 impacts outside of the locking region occurred were completely neglected. For orbits with a larger number of impacts than 100 the first 50 impacts after lift-off were discarded to reduce the influence of transients. It is obvious that the exponents calculated this way have a limited explanatory power for orbits where the maximum number of impacts between two sticking processes is not very high, as in the case of the orbits shown in Fig. 2. For lower dissipation and higher accelerations, sticking orbits are typically much longer.

In Fig. 3(a) bifurcation diagram for $\epsilon = 0.94$ is presented together with the corresponding Lyapunov exponents. The sticking orbits shown there consist of sequences of up to many thousand free jumps. Features which are known from free orbits, such as the symmetry around a baseline, are consequentially reproduced much better.

Whenever Lyapunov exponents could be calculated for sticking solutions in the parameter range from $\epsilon = 0$ to $\epsilon = 0.99$ and $\Gamma = 0$ to $\Gamma = 8$ without violating the criterion given above, we found a positive sign for σ_2. This permits the following conclusion: sticking solutions, at least those consisting of longer series of free jumps, typically diverge exponentially between sticking processes. If the locking region is large enough and the number of free jumps small enough, the ball will get stuck again before the divergence of neighboring trajectories becomes dominating. In this case, sticking solutions will appear periodic, except for small deviations.

For very long sequences of jumps divergence will prevail. In fact, a closer examination of the sticking orbits in Fig. 3(a) reveals that the number of jumps between two sticking processes varies between a few hundreds and a couple of thousands for the same orbit. In numerical calculations periodicity is no longer present. We can even suspect the bulk of the seemingly chaotic orbits in Fig. 3(a) to consist of sticking orbits where the ball has not got stuck yet. This suspicion is confirmed, if the number of iterations is step by step lowered (down to 5000) or increased (up to 100 000). The number of chaotic orbits likewise decreases or increases, whereas the number of sticking orbits increases or decreases. Luck and Mehta [1993] have argued for an exponential relationship between the number of iterations and the probability of the ball to get stuck in this case.

Finally, we once again want to point out that this effect is only due to small numerical errors which can never be avoided. From a analytical point of view, sticking solutions must always be periodical. However, Kowalik *et al.* [1988] could observe a similar behavior experimentally and have shaped the term "self-reanimating chaos" for it, which we will adopt. Of course, in experiments small deviations from initial conditions are always present and could play a role similar to numerical errors in the theory. Whenever we speak of chaos or chaotic orbits without explicitly alluding to "self-reanimating" we will assume that the ball does not get stuck (except at most once in a transient regime). The region in parameter space where self-reanimating chaos appears cannot be unambiguously delimited, since the outcome depends on computational precision.

As we are also interested in giving a more general picture of possible scenarios, we scanned the phase space for several values of ϵ by selecting 100 uniformly distributed initial conditions from the trapping region. The resulting long-term solutions for $\epsilon = 0.5$ are shown in Fig. 4. This picture is typical for high and medium range dissipation. For the free solutions in Fig. 4(a), we observe a number of bifurcation trees starting from the one periodic orbits as described in Sec. 2.2.1. In addition, smaller bifurcation trees can be found, which

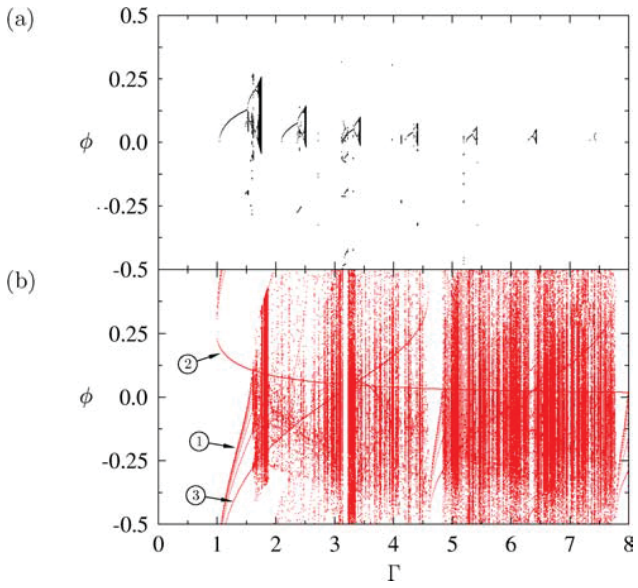

Fig. 4. (a) Bifurcation diagram for $\epsilon = 0.5$. Initial conditions scanned 10×10. (a) Free solutions. (b) Sticking solutions. Explanation of the marked lines: ① the ball gets stuck, ② the ball lifts off, ③ first impact after lift-off.

do not start from period one orbits. Both chaotic and periodic solutions do coexist for some values of γ and ϵ depending on the initial conditions in Fig. 4(a). The same holds true for the sticking solutions shown in Fig. 4(b) which do coexist with free solutions in large regions of parameter space. They follow a pattern of seemingly more regular regions (e.g. after $\Gamma \approx 4.60$ and $\Gamma \approx 7.79$) followed by rather irregular motion. For an interpretation of this structuring we refer the reader to Sec. 4.3.

For increasing values of the coefficient of restitution period one orbits and bifurcation trees move closer and closer and eventually "coalesce" (cf. [Celaschi & Zimmermann, 1987]). Moreover, for low dissipation sticking solutions set in before the period doubling route can develop fully, as in Fig. 3(a). These consist of long sequences of jumps and fill out large parts of parameter space. More details will be given in the following sections.

3.2. *Attractors*

In Fig. 5 we give detailed views of an attractor for $\epsilon = 0.5$ and $\Gamma = 1.75$, for which no sticking occurs in the long-term limit. This has been verified by numerically calculating up to one million impacts for orbits on the attractor. Less detailed pictures of similar attractors can be found in the papers by Celaschi and Zimmermann [1987] and

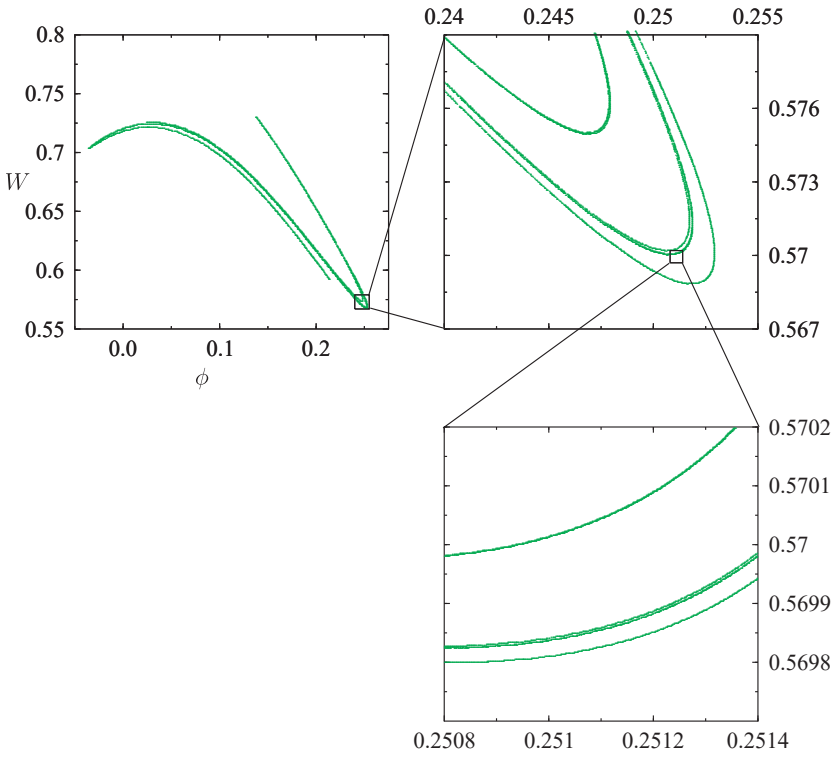

Fig. 5. Fractal composition of the attractor for $\epsilon = 0.5$ and $\Gamma = 1.75$. $\phi_0 = 0.25$, $W_0 = 0$. Structures can be found at arbitrary small scales.

Tufillaro *et al.* [1992]. These attractors are apparently fractal. Attractors for the self-reanimating chaos have been calculated by Luck and Mehta [1993]. Their graphs could be reproduced by us successfully. The structure of these attractors appears to be fractal, too. The same holds true for next impact maps, which we also calculated (see [Tufillaro, 1994a] for an example). We did not determine fractal dimensions or other more tangible criteria to verify fractal properties of attractors or next impact maps. This remains a task for future work.

Nonetheless, it is possible to distinguish between chaos and "self-reanimating" chaos without relying on fractal properties of the respective attractors. To this aim we refer the reader to Fig. 3 in the paper by Luck and Mehta [1993] for the size of the locking region for $\epsilon = 0.5$. From that figure it is evident that the locking region and the attractor shown in Fig. 5 do not overlap. Extensive checks did show that this is commonly the case for strange attractors appearing at the end of fully developed bifurcation cascades.

It can therefore be concluded that such attractors indeed are chaotic and that chaos in the bouncing ball system does exist. Obviously, Luck and Mehta's assumption that a "typical trajectory will explore its whole phase space and end up in the locking region after a finite number of collisions" does not generally hold for arbitrary values of ϵ and Γ. Only for large ϵ and Γ our numerical studies do confirm Luck and Mehta's results, inasmuch as chaotic regions become smaller and smaller and eventually give way to the "self-reanimating" type of numerical chaos.

3.3. *Basin of attraction*

Several examples of basins of attraction can be found in papers by Isomäki [1989] and Tufillaro *et al.* [1992]. Because these authors only distinguish between regular and sticking solutions, we here give a more complete picture, characterizing also chaotic behavior. The structure of the basin of attraction can be very simple in case of one single global attractor, but also rather complex as in Fig. 6 where we scanned the trapping region and indicated which initial conditions belong to which type of attractor. For $\epsilon = 0.5$ and $\Gamma = 1.45$ in Fig. 6(a) an attractive sticking solution and a periodic point at $(\phi_0, W_0) \approx (0.124, 0.666)$ coexist. If the acceleration is slightly increased to $\Gamma = 1.54$,

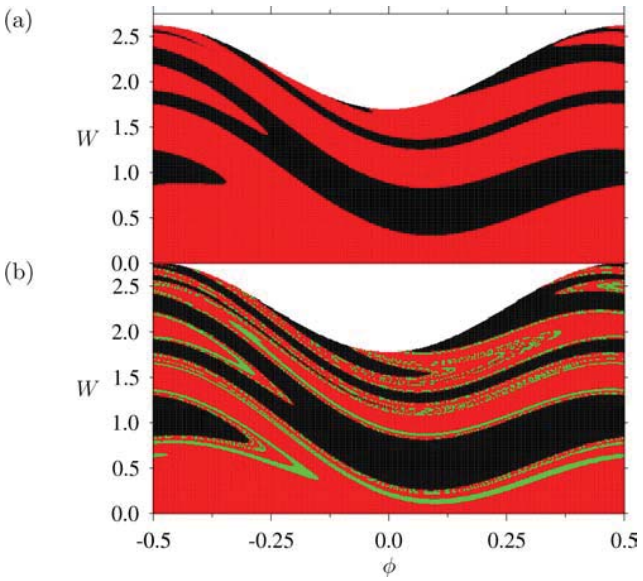

Fig. 6. Basin of attraction for $\epsilon = 0.5$. Black: regular solutions, green: chaotic solutions, red: sticking solutions. (a) $\Gamma = 1.45$. (b) $\Gamma = 1.54$.

the picture shown in Fig. 6(b) results. The sticking solution still exists, but the period one orbit has bifurcated into a period two orbit at $(\phi_0, W_0) \approx (0.157, 0.654)$ and $(\phi_1, W_1) \approx (0.102, 0.679)$. In addition, a chaotic attractor exists. The structure of the basin of attraction is apparently fractal, as could be verified by magnifying cutouts of the graph. The white space in the upper part of Figs. 6(a) and 6(b) does not belong to the trapping region and therefore has not been investigated by us.

3.4. *Global behavior for fixed initial conditions*

If the oscillation of the table is started in its minimum position with the ball at rest, the resulting orbits are of the type shown in Fig. 7(a). Above $\epsilon = 0.99$ we did not acquire any data. Of course, for $\Gamma \leq 1$ the ball sticks to the table forever. But also above $\Gamma = 1$ sticking solutions do prevail. This is not astonishing because of our particular choice of initial conditions. In addition, we observe a number of stable periodic orbits, especially for small ϵ and Γ. These consist mostly of one-periodic orbits and the ensuing bifurcation cascades, followed by chaotic regions.

The large chaotic region in the upper part of the figure is of the self-reanimating type, as we verified by varying the number of iterations (between 10 000 and 100 000). The larger the number of iterations the smaller this region gets.

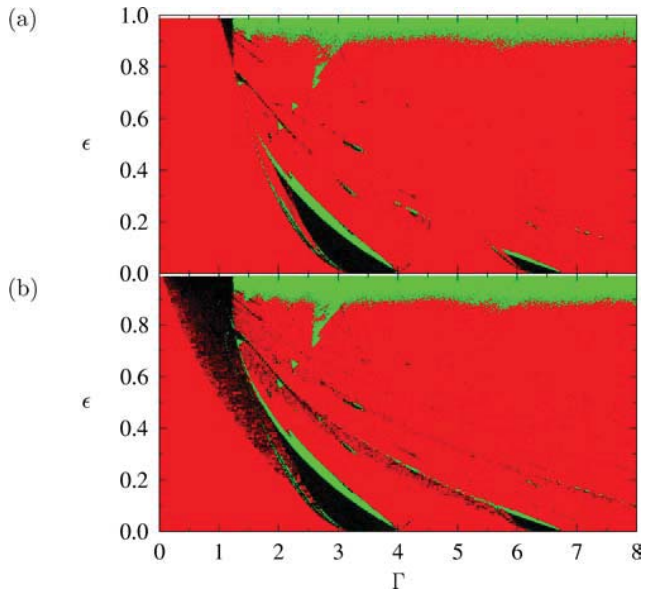

Fig. 7. Long-term behavior of orbits depending on Γ and ϵ. Black: regular solutions, red: sticking solutions, green: chaotic solutions. (a) Fixed initial conditions $\phi_0 = -0.25$, $W_0 = 0$. (b) Fixed initial conditions $\phi_0 = 0$, $W_0 = 125$.

Moreover, self-reanimating chaos is more widespread in the upper part of Fig. 7(b) than in Fig. 7(a). This is in perfect agreement with the remarks made so far, since in Fig. 7(a) initially the ball sticks to the table already once. It is therefore more likely to get caught a second time before the maximum number of calculations is reached than in Fig. 7(b), where we have chosen a rather high initial velocity, slightly above the long-term maximum velocity which we have determined numerically for $\epsilon = 0.99$ and $\Gamma = 8$ by scanning the trapping region.

Another salient difference between the two graphs consists in the large number of periodic orbits for $\Gamma < 1$ in Fig. 7(b). Other features, especially for lower ϵ are comparatively similar.

3.5. *Global behavior for scanned initial conditions*

To get a more complete picture of the solution structure it is necessary to vary the initial conditions on a broader scale. For this purpose we choose 100 different, uniformly distributed initial conditions from the trapping region and register which different types of solution occur for different values of ϵ and Γ. The result is shown in Fig. 8, where we also indicate the lower border of the region of stability of one-periodic solutions, which can be calculated

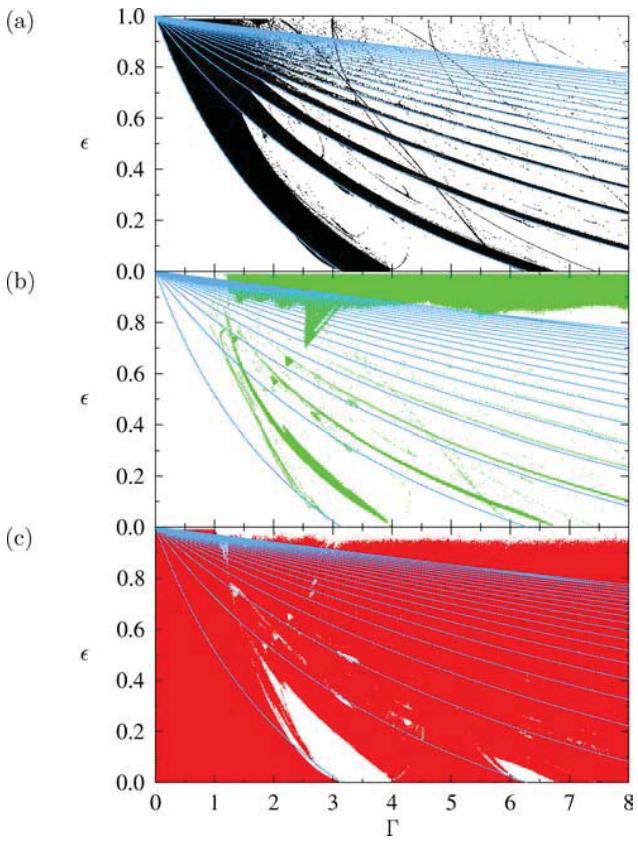

Fig. 8. Possible types of solutions. Initial conditions scanned 10×10. Blue lines indicate the lower border of the region of stability for one-periodic solutions. (a) Periodic solutions. (b) Chaotic solutions. (c) Sticking solutions.

from Eq. (8)

$$\epsilon = \frac{\pi m - \Gamma}{\pi m + \Gamma}. \tag{20}$$

The finger-like structure in Fig. 8(a) results from period-one orbits and the ensuing bifurcation cascades. The chaotic orbits in Fig. 8(b) play a rather subordinate role, if the self-reanimating chaos for large values of ϵ is not taken into account. As can be seen from Fig. 8(c), sticking solutions are by far dominating. They exist in the largest part of parameter space and are mostly globally stable. For increasing Γ this effect can at least be qualitatively understood. Let us suppose that due to a small disturbance (e.g., a numerical inaccuracy) the ball takes off a little later. If the table is oscillating very quickly, the next impact will be at a much later phase than for slow oscillations. For periodic solutions the ball is thus more likely to leave the region of stability. For chaotic solutions the ball will visit a vaster portion of phase space so that the probability of ending up in the locking region increases.

4. Velocity Dependent Coefficient of Restitution

4.1. *Model*

From experiments [Raman, 1918, 1920; Tabor, 1948; Goldsmith, 1960; Bernstein, 1977; Maurone & Wunderlich, 1978; Maurone, 1979; Brody, 1979; Smith *et al.*, 1981; Reed, 1985; Falcon *et al.*, 1998; Gugan, 2000; Stensgaard & Lægsgaard, 2001; Leconte *et al.*, 2006] it is known that the coefficient of restitution ϵ should generally depend on the impact velocity $w' = v'_i - s_i$ measured relatively to the table.

On the one hand, it is generally accepted that a number of different physical effects contribute to this dependence. For example, energy is transfered from the ball to the table on impact by exciting various vibrational modes of the table. This effect can only be neglected, if the thickness of the table is large compared to the diameter of the ball. Other energy loss mechanisms include elastic and viscoelastic waves as well as plastic deformations of the ball or the table [Reed, 1985; Johnson, 1996; Falcon *et al.*, 1998]. On the other hand, competing, sometimes even contradictory theories do exist which describe the dependence of ϵ on w' (compare [Tabor, 1948; Goldsmith, 1960; Johnson, 1996; Falcon *et al.*, 1998; Reed, 1985]). This is due to the fact that the underlying energy dissipation processes are rather complex and depend heavily on the material properties of the ball and the table.

We therefore use data from an experiment by Stensgaard and Lægsgaard [2001] for a steel ball bouncing on a smooth steel block. The most relevant of their findings for our purposes is reproduced in Fig. 9 and indicates that for increasing impact velocity the coefficient of restitution ϵ crosses over from a constant to a behavior decreasing with the impact velocity. We approximate the data points by a constant value $\epsilon_0 = 0.94$ for $|w'| \leq |w'_g| = 0.19\,\mathrm{m/s}$ and by a linear fit for $|w'_g| < |w'| \leq 1.0\,\mathrm{m/s}$. As results from most experiments cited above suggest, an increase in energy dissipation at higher impact velocities is generic for most materials and also for velocities well above $|w'| = 1.0\,\mathrm{m/s}$. Since beyond this point no reliable interpolation can be made based on the experimental data by Stensgaard and Lægsgaard [2001], we immediately interrupted our calculations, if $|w'|$ exceeded $1.0\,\mathrm{m/s}$.

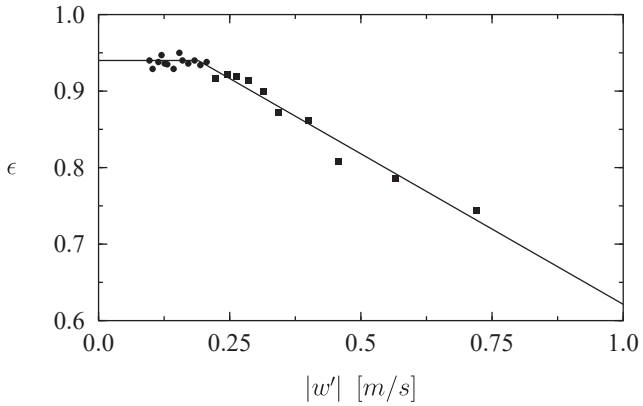

Fig. 9. Dependence of the coefficient of restitution ϵ on the impact velocity for a steel ball bouncing on a steel block. Marked data points from Stensgaard and Lægsgaard [2001]. Straight lines indicate a piecewise linear fit of the data used for our modeling.

By introducing the step function Θ the functional dependence of the coefficient of restitution ϵ can be expressed in a compact way

$$\epsilon(w'_{i+1}) = \epsilon_0[1 + \kappa\Theta(w'_g - w'_{i+1})(w'_{i+1} - w'_g)], \tag{21}$$

where $\kappa = 0.42$ s/m. The basic equation (6) of the bouncing ball problem remains unchanged, whereas Eq. (7) now becomes

$$\begin{aligned} W_{i+1} &= -\epsilon(W'_{i+1})\left\{W_i - 2(\phi_{i+1} - \phi_i)\right. \\ &\quad \left. + \frac{\Gamma}{\pi}[\cos(2\pi\phi_i) - \cos(2\pi\phi_{i+1})]\right\} \\ &= -\epsilon_0\left[1 + \frac{\pi g}{\omega}\kappa\,\Theta(W'_g - W'_{i+1})\right. \\ &\quad \left. \times (W'_{i+1} - W'_g)\right]\left\{W_i - 2(\phi_{i+1} - \phi_i)\right. \\ &\quad \left. + \frac{\Gamma}{\pi}[\cos(2\pi\phi_i) - \cos(2\pi\phi_{i+1})]\right\}. \end{aligned} \tag{22}$$

Since W_{i+1} is decreasing quadratically for $|W'_{i+1}| > (1/\kappa - w'_g)\omega/2\pi g$, it is possible to delimitate the trapping region even further. We will not demonstrate this, since it is only of interest for the particular model discussed here. Finally, from Eq. (22) it is evident that from now on, it is necessary to take into account ω or equivalently the frequency f of the oscillations as an additional parameter. We exemplarily focus on $f = 10\,\mathrm{Hz}$ and $f = 20\,\mathrm{Hz}$ for the remainder of our study.

4.2. *Bifurcation diagrams and Lyapunov exponents*

To obtain Figs. 10 and 11 we have initiated the sequence of jumps at the same phase and with the same velocity as in Fig. 3. A comparison of all three figures clearly shows that the outcome is altered drastically. For velocity-dependent ϵ, self-reanimating chaos becomes dominant at considerably larger values of γ. Even before it sets in, changes are crucial. For example, in Fig. 10(a) a bifurcation cascade can be found at about $\Gamma = 1.5$ which starts from an orbit of period three and which is not present in Fig. 3(a) at all. Generally, alterations are more pronounced for $f = 20\,\text{Hz}$. This could be expected, since velocities are expressed in units of π/ω. A given impact speed W' thus corresponds to a higher unscaled impact speed w' for low frequencies than for high frequencies and the coefficient of restitution ϵ depends on unscaled quantities.

From Fig. 8, it can be inferred that for small values of constant ϵ, periodic and chaotic orbits are more likely to be stable. It can therefore be suspected that in the velocity-dependent case, periodic and chaotic solutions are more widespread, since the "average" coefficient of restitution is lowered. This effect should be more salient for low frequencies. In fact, this point can be corroborated by calculating

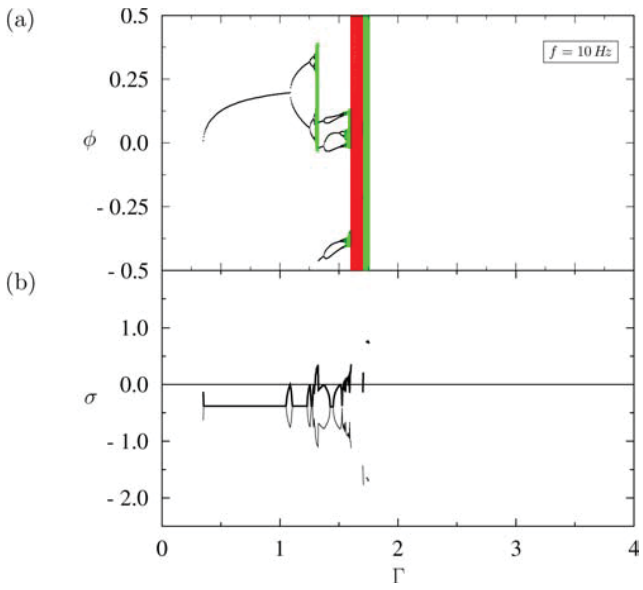

Fig. 10. (a) Bifurcation diagram for $\epsilon_0 = 0.94$ and $f = 10\,\text{Hz}$. Black: regular solutions, red: sticking solutions, green: chaotic solutions. $\phi_0 = 0$, $W_0 = 0.9582$ at $\Gamma = 0.35$. (b) Lyapunov exponents σ_1 ——, σ_2 ——. Also shown is the zero-line.

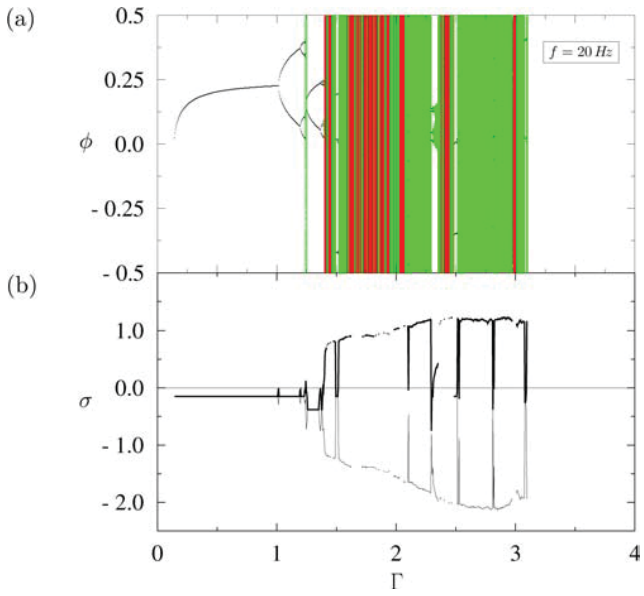

Fig. 11. (a) Bifurcation diagram for $\epsilon_0 = 0.94$ and $f = 20\,\text{Hz}$. Black: regular solutions, red: sticking solutions, green: chaotic solutions. $\phi_0 = 0$, $W_0 = 0.9582$ at $\Gamma = 0.35$. (b) Lyapunov exponents σ_1 ——, σ_2 ——. Also shown is the zero-line.

scanned bifurcation diagrams as in Fig. 4 (which are not shown here) and by the global solution structure which will be treated in the following sections.

4.3. *Global behavior for fixed initial conditions*

To obtain a general picture of the dynamics we first need to model the velocity dependence of the coefficient of restitution for arbitrary values of $\epsilon_0 = \epsilon(w' = 0)$. We proceed exactly as in Sec. 4.1, i.e. for $|w'_i| \leq 0.19\,\text{m/s}$ we fix ϵ at a constant value of ϵ_0 ranging from zero to 0.99 and assume a linear decay for $0.19\,\text{m/s} < |w'| \leq 1.0\,\text{m/s}$. Whenever ϵ becomes negative, we interrupt our calculations. Especially for very low values of ϵ_0 this model is probably not very accurate. However, we are primarily interested in finding out whether the velocity dependence of the coefficient of restitution has significant effects at all. To this aim our simple model is sufficient.

For the same fixed initial conditions $(\phi_0, W_0) = (-0.25, 0)$ as in Fig. 7 we present the resulting types of long-term solution depending on Γ and ϵ_0 for $f = 10\,\text{Hz}$ in Fig. 12(a) and for $f = 20\,\text{Hz}$ in Fig. 13(a). White regions indicate where calculations were interrupted because of a physically impossible negative coefficient of restitution. As a first important point it should be noted, that the size of the region where periodic and chaotic

solutions exist is enlarged in comparison to the case of a constant coefficient of resolution as in Sec. 3.4. As expected, this effect is more pronounced for $f = 10\,\mathrm{Hz}$.

Secondly, it is noteworthy that around $\Gamma = 4.6$ and $\Gamma = 7.8$ isolated columns of sticking solutions do exist for $f = 10\,\mathrm{Hz}$. For $f = 20\,\mathrm{Hz}$ peaks can be found at the same positions, too. This is due to orbits, where the velocities of the ball and the table are equal or almost equal immediately at the first impact after lift-off. The position of the orbits where the ball gets caught without rebouncing at all can be easily determined: The lift-off velocity of the ball after getting stuck amounts to

$$V_l = \frac{\Gamma}{\pi} \cos \arcsin \frac{1}{\Gamma} = \frac{\sqrt{\Gamma^2 - 1}}{\pi}. \qquad (23)$$

In order for the ball and the table to have the same velocity at the first impact after lift-off it is necessary that $V_l = \Delta\tau = (n + 1/2)/2 + \arcsin(1/\Gamma)/2\pi$ or

$$0 = \arcsin \frac{1}{\Gamma} + \sqrt{\Gamma^2 - 1} - \pi\left(n + \frac{1}{2}\right). \qquad (24)$$

This equation can be solved numerically. For $n = 1$ one obtains $\Gamma \approx 4.60$ and for $n = 2$ the result is $\Gamma \approx 7.79$. Moreover,the existence of these orbits explains for the stripes of more regular regions in the bifurcation diagram, Fig. 4(b), which do also exist for other values of ϵ at the same positions.

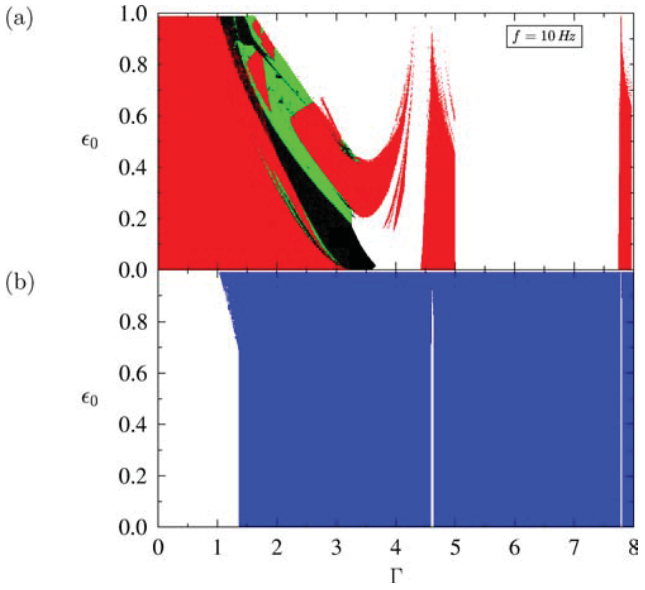

Fig. 12. (a) Long-term behavior depending on Γ and ϵ_0 for $f = 10\,\mathrm{Hz}$, $\phi_0 = -0.25$, $W_0 = 0$. Black: regular solutions, red: sticking solutions, green: chaotic solutions. (b) Regions where the coefficient of restitution ϵ becomes velocity dependent.

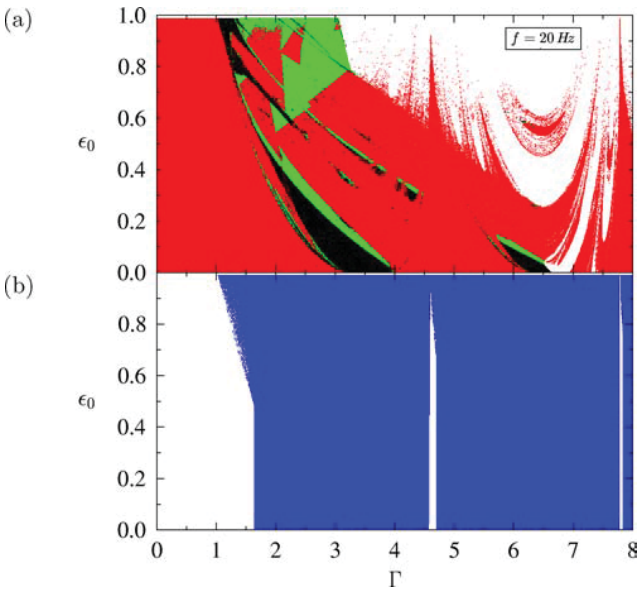

Fig. 13. (a) Long-term behavior depending on Γ and ϵ_0 for $f = 20\,\mathrm{Hz}$, $\phi_0 = -0.25$, $W_0 = 0$. Black: regular solutions, red: sticking solutions, green: chaotic solutions. (b) Regions where the coefficient of restitution ϵ becomes velocity dependent.

In Figs. 12(b) and 13(b) we have indicated the regions in parameter space where the velocity dependence of ϵ actually becomes effective. Here, the orbits around $\Gamma \approx 4.60$ and $\Gamma \approx 7.79$, where the ball gets caught tangentially or almost tangentially, can clearly be discerned again. For high and medium range dissipation the transition from constant to velocity dependent behavior close to $\Gamma = 1.5$ for $f = 20\,\mathrm{Hz}$, respectively $\Gamma = 1.7$ for $f = 20\,\mathrm{Hz}$, does not depend on ϵ_0. This effect stems from sticking solutions, where the ball lifts off and is caught in the same cycle of the table's oscillations. In such a case the impact speed has its highest value at the first impact after lift-off and depends solely on the driving of the table.

4.4. *Global behavior for scanned initial conditions*

As in the case of the velocity independent coefficient of restitution a complete picture of possible scenarios can be obtained by scanning parameters and initial conditions. We present the results for $f = 20\,\mathrm{Hz}$ in Fig. 14. To limit computational time only 20 000 impacts, of which the first 3000 were discarded, are taken into account. In contrast to Figs. 12(b) and 13(b), in Fig. 14(d) only orbits are indicated

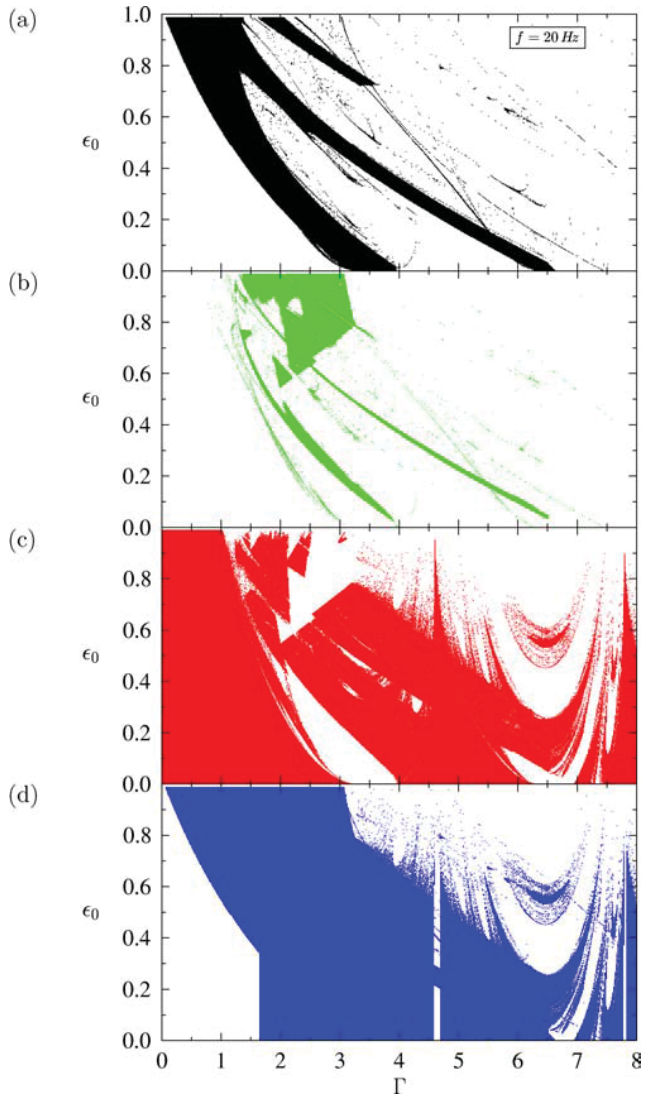

Fig. 14. Possible types of solutions for $f = 20\,\mathrm{Hz}$. Initial conditions scanned 10×10. (a) Periodic solutions. (b) Chaotic solutions. (c) Sticking solutions. (d) Regions where the coefficient of restitution ϵ becomes velocity dependent.

where the coefficient of restitution becomes velocity dependent after the first 3000 iterations have passed, because due to the scanning process everywhere orbits exist for which the impact velocity at the very first impacts is high. As a consequence, white areas in the figure indicate either that for all orbits (with the same Γ and ϵ, but different initial conditions) calculations were interrupted, because $|w'|$ exceeded 1.0 m/s, or that the coefficient of restitution is constant for all surviving orbits. Colored areas indicate that ϵ is velocity dependent for at least one of the scanned orbits beyond the first 3000 impacts.

From Fig. 14 it can be seen that the size of regions with stable chaotic and periodic solutions grows. For small frequencies this effect is more pronounced, as we could see from equivalent graphs for $f = 10\,\mathrm{Hz}$.

Generally speaking, deviations are grave, which brings us to the conclusion that the velocity dependence of the coefficient of restitution cannot be neglected in more realistic models. Qualitatively speaking, this result remains valid, if instead air friction is taken into account, as has been shown by Naylor *et al.* [2002].

5. Jump Heights

The bouncing ball system has also attracted increasing attention as a starting point for understanding the more complicated problem of particle transport on vibrating conveyor belts, where particles are subject to a combined horizontal and vertical oscillation [Rademacher & ter Borg, 1994; Sloot & Kruyt, 1996; Landwehr *et al.*, 1997; El hor & Linz, 2005]. An important characteristic in such technical applications is the transport velocity of the particles. Since this property cannot be determined directly in the bouncing ball system, we examined the property of a similar but accessible quantity, namely the average jump height of the ball. In Fig. 15 the results for the same orbits as in the bifurcation diagrams 3(a), 10(a), and 11(a) are presented.

We made use of three different methods to calculate the jump heights. First, the maximum height of the ball between impacts was consecutively determined. The black lines in Fig. 15 show the averaged value and thus provide information about the absolute average jump height. If each time the position of the table is subtracted from the maximum height of the ball, one determines the average height of the ball relative to the table (the blue lines in Fig. 15). In both of the above cases only jumps were taken into account, where a real maximum of the parabolic trajectory of the ball occurred, in order to avoid the problem of convergence for sticking solutions (where an infinite number of smaller and smaller jumps occurs). Such maximum heights of the ball might be easier to measure in experiments. However, if small jumps without real maxima occur, these will be missed.

The most detailed information is provided by the red line in Fig. 15. To obtain it, the continuous time-average of the height of the ball above the

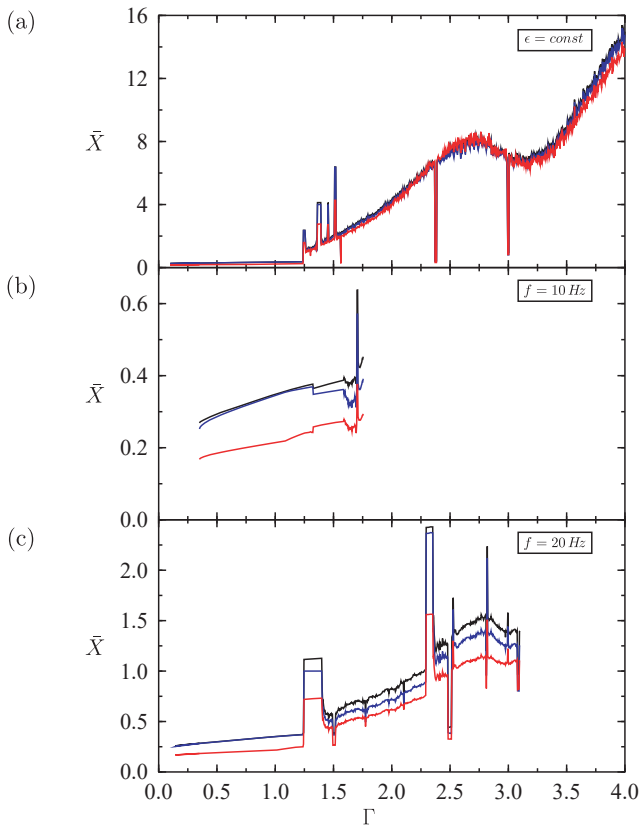

Fig. 15. Average normalized jump height $\overline{X}$ for $\epsilon_0 = 0.94$. Black: absolute height, blue: relative height, red: time average. (a) Constant ϵ as in Fig. 3. (b) $f = 10\,\mathrm{Hz}$ as in Fig. 10. (c) $f = 20\,\mathrm{Hz}$ as in Fig. 11.

table was calculated (the area between the trajectories of the ball and the table in a $t - X$ diagram divided by the time elapsed). As can be seen from the figure, all three methods qualitatively yield the same results.

Generally, it can be said that jump heights vary rather slowly, as long as the ball is moving on the same type of attractor. This even holds true when an attractor bifurcates, as e.g. the period one orbit at $\Gamma \approx 1.0$ in Fig. 3(a), and when a transition from periodic to chaotic behavior takes place (as can be seen in other parameter regimes which we do not show here). In this sense jump heights are therefore less sensitive than Lyapunov exponents.

Finally, it is not obvious for which types of solution the jump heights are higher. All upward and downward peaks in Fig. 15 belong to periodic or chaotic solutions. Jump heights for sticking solutions fluctuate, too, but around a base line, which shows a nonmonotonous behavior. Steep downward peaks can be found at the strictly periodic regions given by $0 = \arcsin(1/\Gamma) + \sqrt{\Gamma^2 - 1} - \pi(n + 1/2)$ (cf. Sec. 4.4). These are not visible in Fig. 15.

As can be expected, for velocity dependent ϵ deviations are more pronounced in dimensionless units for small frequencies.

6. Conclusion

In this paper, we have studied in considerable detail two models for the bouncing ball system. We have started out by reviewing the standard theoretical model which neglects a number of physical effects. Such effects can be expected to be of significance in experiments. As a first important result, the hitherto contentious question of the existence of chaos in the bouncing ball system could be answered in a positive way. We found out that Lyapunov exponents alone are not sufficient to distinguish between chaotic and sticking solutions because of the existence of so-called self-reanimating chaos. However, attractors with positive Lyapunov exponents do exist which are confined to restricted parts of phase space that do not overlap with the locking regions. Orbits that lie on such attractors are therefore chaotic and in this case the ball will not stick to the table. A detailed investigation of the long-term behavior depending on parameters and initial conditions has shown that on the whole such chaotic solutions play a rather subordinate role. In the larger part of parameter space sticking solutions prevail, especially for small energy dissipation and high accelerations.

To make the model more realistic, the velocity dependence of the coefficient of restitution has been included in the theoretical description. In consequence, the same types of solutions as before can be found, namely periodic, chaotic and sticking solutions. However, significant changes take place that affect single orbits and alter the overall picture drastically. Generally speaking, the region of stability of chaotic and periodic solutions in parameter space grows. In addition, average jump heights of the ball have been examined. These can depend very sensitively on small variations of parameters.

Finally, for future work it is of primary importance to model the velocity dependence of the coefficient of restitution more accurately for high and medium range dissipations. As a next step, it would be instructive to include the influence of other effects such as air friction, rotational degrees of freedom, rough table surfaces, and so on. Other questions, for example, the remarkable fluctuations of

the average jump height, deserve to be investigated in more detail in future studies.

References

Bernstein, A. D. [1977] "Listening to the coefficient of restitution," *Am. J. Phys.* **45**, 41.

Brody, H. [1979] "Physics of the tennis racket," *Am. J. Phys.* **47**, 482.

Celaschi, S. & Zimmermann, R. L. [1987] "Evolution of a two-parameter chaotic dynamics from universal attractors," *Phys. Lett. A* **120**, 447.

de Oliveira, C. R. & Gonçalves, P. S. [1997] "Bifurcations and chaos for the quasiperiodic bouncing ball," *Phys. Rev. E* **56**, 4868.

El hor, H. & Linz, S. J. [2005] "Model for transport of granular matter on an annular vibratory conveyor," *J. Stat. Mech.*, L02005.

Everson, R. M. [1986] "Chaotic dynamics of a bouncing ball," *Physica D* **19**, 355.

Falcon, E., Laroche, C., Fauve, S. & Coste, C. [1998] "Behavior of one inelastic ball bouncing repeatedly of the ground," *Eur. Phys. J. B* **3**, 45.

Fermi, E. [1949] "On the origin of the cosmic radiation," *Phys. Rev.* **75**, 1169.

Goldsmith, W. [1960] *Impact: The Theory and Physical Behavior of Colliding Solids* (Edward Arnold, London).

Gugan, D. [2000] "Inelastic collision and the Hertz theory of impact," *Am. J. Phys.* **68**, 920.

Hansen, L.-U. W., Christensen, M. & Mosekilde, E. [1995] "Deterministic analysis of the probability machine," *Phys. Scripta* **51**, 35.

Hénon, M. [1976] "A two-dimensional mapping with a strange attractor," *Commun. Math. Phys.* **50**, 69.

Isomäki, H. M. [1989] "Fractal properties of the bouncing-ball dynamics," *Nonlinear Dynamics in Engineering Systems*, ed. Schiehlen, W., p. 125.

Johnson, K. [1996] *Contact Mechanics* (Cambridge Univ. Press, Cambridge).

Klein, M. [1992] "Untersuchung chaotischer Attraktoren und fraktaler Strukturen in nichtlinearen dynamischen Systemen: Von der chaotischen Hierarchie über fraktale Bistabilituät zum Kugelchaos," PhD thesis, Eberhard-Karls-Universität Tübingen.

Kowalik, Z. J., Franaszek, M. & Pierański, P. [1988] "Self-reanimating chaos in the bouncing-ball system," *Phys. Rev. A* **37**, 4016.

Landwehr, F., Lange, R. & Walzel, P. [1997] "Partikeltransport unter verschiedenen Stoßbedingungen auf vibrierten Unterlagen," *Chemie Ingenieur Technik* **69**, 1422.

Leconte, M. Y. G., Palencia, F., Lecoutre, C., Evesque, P. & Beysens, D. [2006] "Inelastic ball-plane impact: An accurate way to measure the normal resitution coefficient," *Appl. Phys. Lett.* **89**, 243518.

Lichtenberg, A., Liebermann, M. & Cohen, R. [1980] "Fermi acceleration revisited," *Physica D* **1**, 291.

Luck, J. M. & Mehta, A. [1993] "Bouncing ball with a finite restitution: Chattering, locking, and chaos," *Phys. Rev. E* **48**, 3988.

Luna-Acosta, G. A. [1990] "Regular and chaotic dynamics of the damped Fermi accelerator," *Phys. Rev. A* **42**, 7155.

Maurone, P. A. & Wunderlich, F. J. [1978] "Bouncing ball experiment," *Am. J. Phys.* **46**, 413.

Maurone, P. A. [1979] "Time of flight for the bouncing ball experiment," *Am. J. Phys.* **47**, 560.

Mehta, A. & Luck, J. M. [1990] "Novel temporal behavior of a nonlinear dynamical system: The completely inelastic bouncing ball," *Phys. Rev. Lett.* **65**, 393.

Mello, T. M. & Tufillaro, N. B. [1987] "Strange attractors of a bouncing ball," *Am. J. Phys.* **55**, 316.

Naylor, M. A., Sánchez, P. & Swift, P. [2002] "Chaotic dynamics of an air-damped bouncing ball," *Phys. Rev. E* **66**, 057201.

Pierański, P., Kowalik, Z. & Franaszek, M. [1985] "Jumping particle model. A study of the phase space of a non-linear dynamical system below its transition to chaos," *J. Physique* **46**, 681.

Pierański, P. & Malecki, J. [1986] "Noisy precursors and resonant properties of the period-doubling modes in a nonlinear dynamical system," *Phys. Rev. A* **34**, 582.

Pierański, P. [1988] "Direct evidence for the suppression of period doubling in the bouncing-ball system," *Phys. Rev. A* **37**, 1782.

Pippard, A. B. [1989] *The Physics of Vibration*, Vol. 1 (Cambridge Univ. Press, Cambridge), first published 1979.

Rademacher, F. J. C. & ter Borg, L. [1994] "On the theoretical and experimental conveying speed of granular bulk solids on vibratory conveyors," *Eng. Res.* **60**, 261.

Raman, C. V. [1918] "The photographic study of impact at minimal velocities," *Phys. Rev.* **12**, 442.

Raman, C. V. [1920] "On some applications of Hertz's theory of impact," *Phys. Rev.* **15**, 277.

Reed, J. [1985] "Energy loss due to elastic wave propagation during an elastic impact," *J. Phys. D* **18**, 2329.

Sloot, E. M. & Kruyt, N. P. [1996] "Theoretical and experimental study of the transport of granular materials by inclined vibratory conveyors," *Powder Technol.* **87**, 203.

Smith, P. A., Spencer, C. D. & Jones, D. E. [1981] "Microcomputer listens to the coefficient of restitution," *Am. J. Phys.* **49**, 136.

Stensgaard, I. & Lægsgaard, E. [2001] "Listening to the coefficient of restitution revisited," *Am. J. Phys.* **69**, 301.

Stöckmann, H.-J. [2007] *Quantum Chaos: An Introduction* (Cambridge Univ. Press, Cambridge).

Tabor, D. [1948] "A simple theory of static and dynamic hardness," *Proc. Roy. Soc. A* **192**, 247.

Tufillaro, N. & Albano, A. [1986] "Chaotic dynamics of a bouncing ball," *Am. J. Phys.* **54**, 939.

Tufillaro, N., Mello, T. M., Choi, Y. M. & Albano, A. [1986] "Period doubling boundaries of a bouncing ball," *J. Physique* **47**, 1477.

Tufillaro, N. B., Abbott, T. & Reilly, J. [1992] *An Experimental Approach to Nonlinear Dynamics and Chaos* (Adison-Wesley, Redwood City, CA).

Tufillaro, N. B. [1994a] "Braid analysis of a bouncing ball," *Phys. Rev. E* **50**, 4509.

Tufillaro, N. B. [1994b] "Comment on 'bouncing ball with finite restitution: Chattering, locking, and chaos'," arXiv:chao-dyn/9411009 v2 15 Nov 1994.

Vargas, M. C., Huerta, D. A. & Sosa, V. [2009] "Chaos control: The problem of a bouncing ball revisited," *Am. J. Phys.* **77**, 857.

Zaslavskii, G. M. [1978] "The simplest case of a strange attractor," *Phys. Lett. A* **69**, 145.

Zimmermann, R. L., Celaschi, S. & Neto, L. G. [1992] "The electronic bouncing ball," *Am. J. Phys.* **60**, 370.